2007

Population Study of the Variation in Monochromatic Aberrations of the Normal Human Eye Over the Central Visual Field

Matthew Sheehan
Technological University Dublin, matthew.sheehan@tudublin.ie

Alexander Goncharov
National University of Ireland, Galway, Ireland

Veronica O'Dwyer
Technological University Dublin, veronica.odwyer@tudublin.ie

See next page for additional authors

Recommended Citation

Sheehan, M.T. et al. (2007) Population study of the variation in monochromatic aberrations of the normal human eye over the central visual field, Opt. Express 15, 7367-7380, doi.org/10.1364/OE.15.007367

Population study of the variation in monochromatic aberrations of the normal human eye over the central visual field

Matthew T. Sheehan[a], Alexander V. Goncharov[b], Veronica M. O'Dwyer[a], Vincent Toal[a], and Christopher Dainty[b]

[a]*Optometry Department, School of Physics, Dublin Institute of Technology, Dublin, Ireland*
marty_sheehan@yahoo.com.au
[b]*Department of Experimental Physics, National University of Ireland, Galway, Ireland*
alexander.goncharov@nuigalway.ie, c.dainty@nuigalway.ie

Abstract: We present data analysis for ocular aberrations of 60 normal eyes measured with a Hartmann-Shack (HS) wavefront sensor (WFS). Aberration measurements were made on-axis and at 5 degree field angles in the nasal, inferior, temporal and superior semi-meridians. Particular attention is given to aberration distributions and possible strategies for aberration correction are discussed. A versatile HS WFS was designed and constructed with features of simultaneous pupil centre determination, off-axis capability, real-time data displays, and efficient lenslet sampling orientation. The subject alignment is achieved by the use of a parallel channel that is recombined with the sensing channel to simultaneously image the eye and the HS spots onto a single CCD. The pupil centre is determined using this image of the eye (iris edge), rather than the HS spots. The optical design includes a square lenslet array positioned with its diagonals aligned with the most typical principal astigmatic meridians of the eye. This favourable orientation helps to enlarge the dynamic range of the WFS. The telecentric re-imaging of the HS spots increases the robustness of the system to defocus in the event of CCD misalignment.

OCIS codes: (170.4460) Ophthalmic Optics; (330.5370) Physiological optics; (330.7310) Vision; (010.1080) Adaptive Optics.

References and links

1. J. Liang, B. Grimm, S. Goelz and J. F. Bille, "Objective measurement of wave aberrations of the human eye with use of a Hartmann-Shack wave-front sensor**,**" J. Opt. Soc. Am. A **11**, 1949-1957 (1994).
2. L.N. Thibos, X. Hong, A. Bradley, and X. Cheng, "Statistical variation of aberration structure and image quality in a normal population of healthy eyes," J. Opt. Soc. Am. A. **19**, 2329-2348 (2002).
3. J. Porter, A. Guirao, I.G. Cox, and D. R. Williams, "Monochromatic aberrations of the human eye in a large population," J. Opt. Soc. Am. A **18**, 1793-1803 (2001).
4. H. Cheng, J. K. Barnett, A. S. Vilupuru, J. D. Marsack, S. Kasthurirangan, R. A. Applegate, A. Roorda, "A population study on changes in wave aberrations with accommodation," J. Vision **4**, 272-280 (2004).
5. A. Guirao and P. Artal, "Off-axis monochromatic aberrations estimated from double pass measurements in the human eye," Vision Res. **39**, 207-217 (1999).
6. L. Lundström, J. Gustafsson, I. Svensson, and P. Unsbo, "Assessment of objective and subjective eccentric refraction," Optom. Vision Sci. **82**, 298-306 (2005).
7. R. Navarro, E. Moreno, and C. Dorronsoro, "Monochromatic aberrations and point-spread functions of the human eye across the visual field," J. Opt. Soc. Am. A **15**, 2522-2529 (1998).
8. D. A. Atchison and D. H. Scott, "Monochromatic aberrations of human eyes in the horizontal visual field," J. Opt. Soc. Am. A **19**, 2180-2184 (2002).
9. D. A. Atchison, D. H. Scott, and W. N. Charman, "Hartmann-Shack technique and refraction across the horizontal visual field," J. Opt. Soc. Am. A **20**, 965-973 (2003).
10. D. A. Atchison, "Anterior corneal and internal contributions to peripheral aberrations of human eyes," J. Opt. Soc. Am. A **21**, 335-359 (2004).

#81814 - $15.00 USD Received 3 Apr 2007; revised 10 May 2007; accepted 25 May 2007; published 31 May 2007

11. M.T. Sheehan, A.V. Goncharov, and J.C. Dainty, "Design of a versatile clinical aberrometer," *Proc. SPIE* **5962,** 59620M, in *Optical Design and Engineering II*, L. Mazuray and R. Wartmann Eds. (2005).
12. A. V. Goncharov and C. Dainty, "Wide-Field Schematic Eye Model with Gradient-Index Lens," accepted for publication in JOSA A.
13. J. Carroll, D.C. Gray, A. Roorda, D.R. Williams, "Recent advances in retinal imaging with adaptive optics," Opt. Photon. News, **16**, 36-42, (2005).
14. L. Thibos, R. A. Applegate, J. T. Schwiegerling, and R. Webb, "Standards for reporting the optical aberrations of eyes," in *Vision Science and its Applications*, OSA Technical Digest, paper SuC1 (2000).
15. C. L. Liang, S.H. Juo, C.J. Chang, "Comparison of higher-order wavefront aberrations with 3 aberrometers," J Cataract Refract Surg **11**, 2153-6 (2005).
16. E. Fernández, A. Unterhuber, P. Prieto, B. Hermann, W. Drexler, and P. Artal, "Ocular aberrations as a function of wavelength in the near infrared measured with a femtosecond laser," Opt. Express **13**, 400-409 (2005).
17. L. Llorente, L. Díaz-Santana, D. Lara-Saucedo, and S. Marcos, "Aberrations of the human eye in visible and near infrared illumination," Optom. Vision Sci. **80**, 26-35 (2003)
18. D. R. Neal, C.D. Baer, and D.M. Topa, "Errors in Zernike transformations and non-modal reconstruction methods," J. Refract. Surg. **21**, 558-562 (2005).
19. L. Lundström and P. Unsbo, "Transformation of Zernike coefficients: scaled, translated, and rotated wavefronts with circular and elliptical pupils," J. Opt. Soc. Am. A **24**, 569-577 (2007).
20. R. I. Calver, M. J. Cox, and D. B. Elliott, "Effect of aging on the monochromatic aberrations of the human eye," J. Opt. Soc. Am. A **16**, 2069-2078 (1999).
21. G. Smith, M. J. Cox, R. Calver, and L. F. Garner, "The spherical aberration of the crystalline lens of the human eye," Vision Res. **41**, 235-243 (2001).
22. S. Amano, Y. Amano, S. Yamagami, T. Miyai, K. Miyata, T. Samejima, and T. Oshika, "Age-related changes in corneal and ocular higher-order wavefront aberrations," Am. J. Ophthalmol. **137**, 988-992 (2004).
23. J. L. Alió, P. Schimchak, H. P. Negri, and R. Montés-Micó, "Crystalline lens optical dysfunction through aging," Ophthalmol. **112**, 2022-2029 (2005).
24. P. Artal and A. Guirao, "Contributions of the cornea and the lens to the aberrations of the human eye," Opt. Lett., **23**, 1713-1715 (1998).
25. P. Artal, A. Guirao, E. Berrio, and D. R. Williams, "Compensation of corneal aberrations by the internal optics in the human eye," J. Vision **1**, 1–8 (2001).
26. P. Artal, E. Berrio, A Guirao, and P. Piers, "Contribution of the cornea and internal surfaces to the change of ocular aberrations," J. Opt. Soc. Am. A **19**, 137-143 (2002).
27. A. Guirao, J. Porter, D. R. Williams, and I. G. Cox, "Calculated impact of higher-order monochromatic aberrations on retinal image quality in a population of human eyes," J. Opt. Soc. Am. A **19**, 620-628 (2002).
28. J. A. M. Jennings, and W. N. Charman, "Off-axis image quality in the human eye," Vision Res. **21**, 445-455 (1981).
29. A. Bradley, and L. N. Thibos, "Modeling off-axis vision - I: the optical effects of decentering visual targets or the eye's entrance pupil," in *Vision Models for Target Detection and Resolution*, E. Peli, ed. (World Scientific Press, 1995), pp. 313-337.
30. S. Bará and R. Navarro, "Wide-field compensation of monochromatic eye aberrations: expected performance and design trade-offs," J. Opt. Soc. Am. A **20**, 1-10 (2003).
31. P. A. Bedggood, R. Ashman, G. Smith, and A. B. Metha, "Multiconjugate adaptive optics applied to an anatomically accurate human eye model," Opt. Express **14**, 8019-8030 (2006).

1. Introduction

Due to the relatively recent development of Hartmann-Shack (HS) aberrometers for the human eye [1], there have been only a few population studies of normal eyes using this technology. A study by Thibos and colleagues is one of the largest in the literature, detailing the statistical variation of higher order aberrations over a 6 mm pupil for 200 eyes [2]. An earlier population study by Porter *et al*. describes the aberration structure of 218 normal human eyes for 5.7 mm pupils [3]. More recently, Cheng *et al.* reported aberration measurements for 74 eyes over a 5 mm pupil as part of their study of ocular aberrations and accommodation [4]. Vision scientists consider it an important fundamental and clinical endeavor to accurately describe the higher order monochromatic aberrations of the healthy normal eye. Ultimately having more experimental data one could better understand the origin of ocular aberrations and their significance to image formation on the retina.

Regarding off-axis aberrations, work by Guirao and Artal has concentrated on off-axis refraction (describing lower order aberrations) and the off-axis modulation transfer function [5]. Unfortunately, there are only a few studies of off-axis ocular aberrations measured using

#81814 - $15.00 USD Received 3 Apr 2007; revised 10 May 2007; accepted 25 May 2007; published 31 May 2007

HS technology. Lundström and colleagues presented their results for off-axis aberration measurements at 20 degrees and 30 degrees eccentricities of the horizontal nasal visual field of 50 eyes using HS technology and other refraction techniques [6]. However, most reports in this field are case studies with measurements performed on only a few subjects. A study by Navarro *et al.* showed off-axis optical quality of the eye for four subjects over 6.7 mm pupils [7]. Atchison and Scott [8], and Atchison *et al*. [9-10] presented their results for off-axis aberration study in five eyes for 6 mm pupils. To enlarge the data available in this area, it was decided to conduct an experiment examining the higher order monochromatic aberrations in a population of normal healthy eyes over the central 10 degree field.

For this purpose we designed and built a versatile HS wavefront sensor (WFS) [11]. It is hoped that this data will aid in the development of wide-field model eyes [12] and designs for multi-directional ocular adaptive optics systems to achieve high-resolution retinal imaging over larger fields [13].

2. Instrument design

A HS WFS was designed to combine useful research features such as real-time data displays, adaptability to new projects, and off-axis capability, with features typical of a clinical instrument such as transportability, compact size and a user-friendly interface. An earlier instrument design [11] was modified to make it suitable for this experiment. The optical layout is shown in Fig 1.

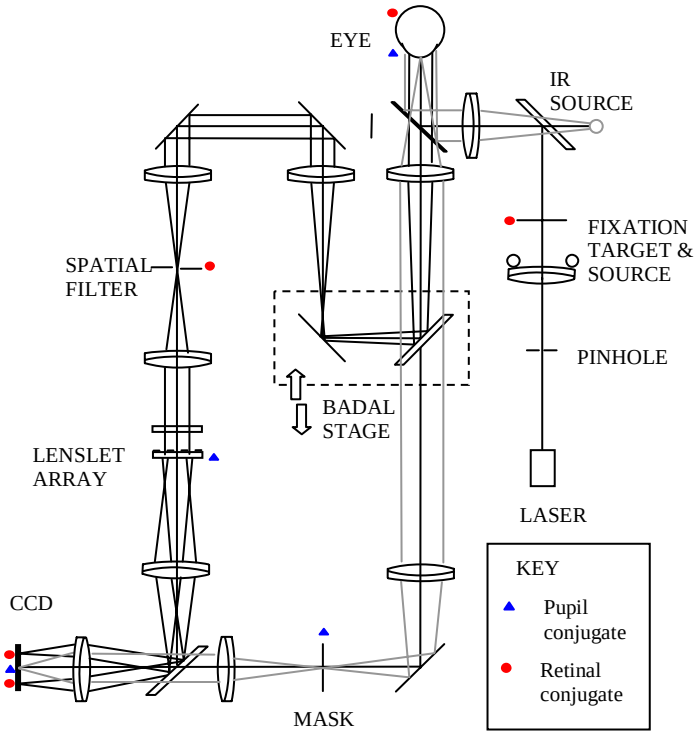

Fig. 1. Optical layout of the versatile HS WFS. Retinal conjugates are shown by a triangle icon. Pupil conjugates are shown by a circle icon.

The unique design features include telecentric imaging of the HS spots, which increases the robustness of the system to defocus in the event of CCD misalignment and has an additional benefit of reduced field curvature. Simultaneous imaging of the eye via the alignment channel allows the pupil centre to be determined independently of the HS spots. The pupil centre is found by analysing the image of the iris with an edge-detection algorithm.

#81814 - $15.00 USD Received 3 Apr 2007; revised 10 May 2007; accepted 25 May 2007; published 31 May 2007

Data points for the iris edge are fitted to a circle by a least squares technique and the centre of this circle is defined as the pupil center. Small errors are associated with this approximation because not all pupils are perfectly circular and this is especially true upon pharmacological dilation.

The Badal is used to correct the 'best sphere' of the refractive error, therefore astigmatism is typically the dominant aberration required to be sensed at the lenslet array. The lenslet array has a 10 mm focal length, 190 micron pitch, and square geometry. It is rotated at 45 degrees to the horizontal meridian of the eye in order to achieve a better sampling and larger dynamic range for astigmatism. It is expected that the majority of astigmatism in the population will be at meridians typically close to either 0 or 90 degrees, rather than at meridians close to 45 or 135 degrees. Therefore, the typical HS spot movement in each subaperture will be close to the vertical or horizontal directions rather than along diagonal directions. Future modifications can be envisaged where the lenslet array has a two (or multiple) rotation-position arrangement and astigmatic dynamic range can be even further enhanced. Due to magnification, the spatial sampling density at the eye is 380 microns and reduces by a factor of 1.41 in the horizontal and vertical meridians. The dynamic range of the WFS transposes to –9.50 to +13.00 diopters spherical (Badal range) and 4.75 diopters cylindrical (lenslet range for a 6 mm pupil).

The retinal beacon is produced with a 677 nm laser diode. The fixation target is a reticule image (black on white) containing predominantly high spatial frequencies. The target provides a 10 degree field to the subject and is back illuminated by 526 nm LEDs. It can be translated along the optical axis and therefore has focusing capability independent of the Badal. A slight curvature in the target compensates for the intrinsic field curvature of the fixation channel.

The alignment channel uses 890 nm LEDs to illuminate the eye. This avoids distracting the subject and altering the state of the eye. The 12 mm field of view provides the examiner with distinguishing landmarks for orientation and the potential to monitor contact lens and/or eyelid properties during aberration measurements. To limit pollution of the HS spots when superimposing the alignment channel image onto the single CCD, an annulus mask is conjugated to the pupil to block out a central zone. This design constrains the measurable the pupil size to diameters between 4 mm and 9.5 mm.

Further details of the the optical, mechanical and electrical assemblies of the experimental HS WFS are described in detail elsewhere [11]. User-friendly software was developed to provide the clinician with data displays at up to 10 Hertz. A personal computer was used to control the instrument and record wavefront measurements.

3. Subject selection

No age limit was set by the subject selection criteria, although young adult university students comprised the majority of volunteers. Subjects were examined to assess their suitability to safely undergo pupil dilation. Subjects with ocular disease (including keratoconus) or history of ocular surgery (including refractive surgery) were excluded. Subjects with cataracts, media opacities, irregular pupil shapes, or dry eye were excluded from the experiment. To allow the pooling and comparison of individual results within the sample, subjects whose dilated pupil diameter was less than 6 mm were excluded. Due to optical design constraints, subjects with dilated pupil diameters greater than 9.5 mm and subjects with refractive errors outside the range of the WFS (–9.50 DS to +13.00 DS / –4.75 DC for a 6mm pupil) were excluded from the study.

Thirty-two volunteers (14 males and 18 females) were recruited and screened according to the subject selection criteria. The refractive errors of subjects ranged from +4.25 DS to -4.00 DS (mean -2.07 DS), and from -0.25 DC to -2.75 DC (mean -0.73 DC). Measurements were performed on both eyes of twenty-eight subjects and only on one eye for four subjects, giving a total of sixty eyes examined. The age of the subjects ranged from 12 years to 57 years (mean 25.7 years). On-axis aberration measurements were performed on all sixty eyes, and off-axis aberration measurements were performed on thirty-one of these eyes. A pharmacological agent (Tropicamide 1%) was used to dilate the subject's pupils and to reduce accomodation fluctuations. Some subjects elected to wear an occluder on the non-test eye

#81814 - $15.00 USD Received 3 Apr 2007; revised 10 May 2007; accepted 25 May 2007; published 31 May 2007

during measurements. The study was conducted with the approval of the Ethics Committee of Dublin Institute of Technology.

4. Pilot study

The first part of the pilot study was conducted on 21 eyes to compare the aberration measurements of our experimental WFS to those of a commercial WFS (ZyWave, Bausch and Lomb). Subjects were selected according to the criteria described in section 3. One drop of 1% Tropicamide was administered to each eye being measured and adequate time was allowed to achieve satisfactory pupil dilation and cycloplegia (loss of accomodation).

The laser power of the experimental WFS was 1.2 microwatts at the eye and the CCD exposure time was 45 milliseconds. The Badal optometer was set at the 'best sphere' value of the subject's refractive error to remove defocus from the sensing channel. Each subject was aligned with the WFS and positioned against a chin-rest and forehead-rest. A bite bar was not used. The subject was asked to fixate the laser in the central area of the fixation target, which thereby aligned the subject's line of sight to the measurement axis of the WFS. The examiner viewed the alignment channel image to make fine adjustments to the subject alignment. The subject was asked to blink and then immediately following the blink, measurements were recorded. For each measurement, twenty images were captured over a typical duration of 2.5 seconds. All measurements were taken in a darkened room. The examiner manually reviewed the image quality, pupil edge detection, and the alignment of the subject. If the spot quality or subject alignment was poor, the results were not used and the measurement was repeated. A computer processed each image to determine the centroids of the HS spots and the edge of the iris. The local slope data was then used to fit the wavefront with Zernike polynomials up to the 5^{th} order by a least squares method over a 6 mm pupil (the analysis of HS spots was restricted to a 3 mm radius from the determined pupil centre). The Zernike coefficients for each mode, were then averaged to produce a single set of coefficients. All results are reported for a 6 mm pupil diameter and according to accepted standards [14].

Immediately following the experimental WFS measurements, subjects were aligned and measured with the ZyWave aberrometer. For each measurement, the ZyWave captures five HS images and selects the 'best' three from which it then generates a set of Zernike coefficients up to 5^{th} order. Zernike coefficients for 6 mm pupil diameters were exported and converted to a standard format [14]. Three successive measurements were averaged per eye to produce a single set of coefficients which were then compared to the experimental WFS results.

All results from the pilot study (part 1) are reported for a 6 mm pupil with defocus Z_2^0 removed. Typical phase maps (2^{nd} to 5^{th} order) are shown in Fig. 2 for six eyes from the pilot study. The Zernike coefficients measured by the ZyWave were subtracted from those measured by the experimental WFS to produce residual phase maps. Fig. 3 shows the residual phase maps of two typical eyes. The wavefront RMS values for subject 7 are 0.62 microns (ZyWave), compared to 0.70 microns (experimental WFS), and the residual RMS is 0.17 microns. If analysis is restricted to the higher order modes (3^{rd} to 5^{th} order) for subject 7, the wavefront RMS values are 0.35 microns (ZyWave), compared to 0.30 microns (experimental WFS), the residual RMS is 0.11 microns. The wavefront RMS values for subject 8 are 0.43 microns (ZyWave), compared to 0.45 microns (experimental WFS), and the residual RMS is 0.14 microns. If analysis is restricted to the higher order modes (3^{rd} to 5^{th} order) for subject 8, the wavefront RMS values are 0.21 microns (ZyWave), compared to 0.21 microns (experimental WFS), and the residual RMS is 0.13 microns.

The residual RMS (2^{nd} to 5^{th} order) was calculated for each individual eye, and then group results were averaged, giving a mean residual RMS of 0.28 microns. If analysis is restricted to higher order aberrations (3^{rd} to 5^{th} order), the mean residual RMS is 0.22 microns. These residual higher order RMS values indicate considerable differences in measurements between the two aberrometers. However, when interpreting these values it is important to note that the measurements were performed on real eyes, and therefore suffer a host of complicating factors (such as temporal fluctuations in aberrations) that are absent in validation studies that

#81814 - $15.00 USD Received 3 Apr 2007; revised 10 May 2007; accepted 25 May 2007; published 31 May 2007

use phase plates or calibrated lenses. Comparing RMS values of the experimental WFS to the ZyWave, the higher order (3^{rd} to 5^{th} order) wavefront RMS is within ± 0.1 micron for over 80% of eyes in our pilot study. This achieves agreement equal to the highest level observed by Liang *et al* in their study comparing three commercial aberrometers [15].

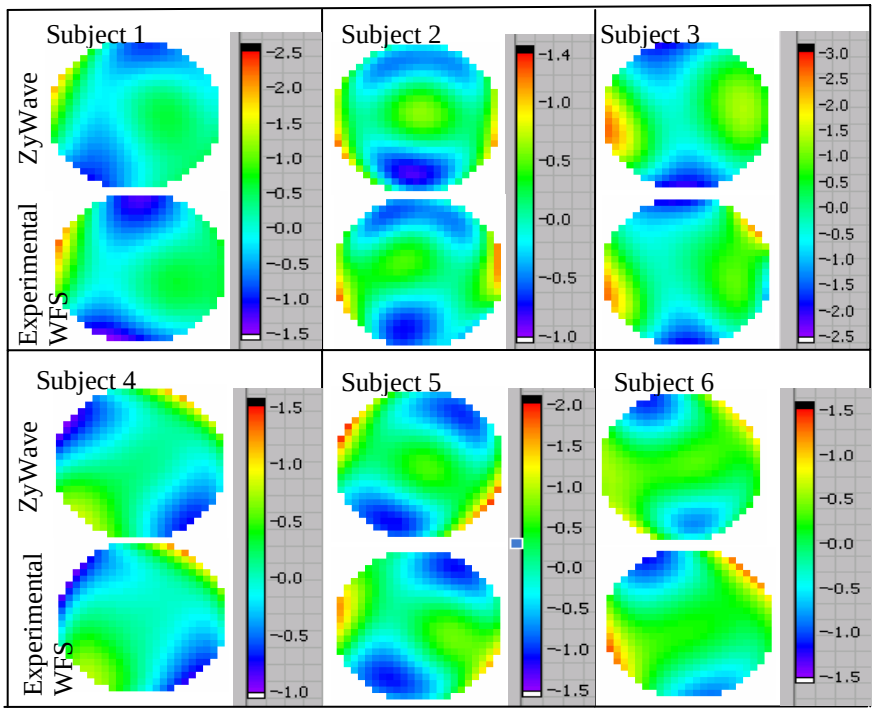

Fig. 2. Phase maps as measured by the ZyWave and the experimental WFS for six eyes over a 6 mm pupil diameter. Defocus Z_2^0 has been removed from the analysis. The colour scales represent wavefront phase (microns) and are consistent within each pair of results.

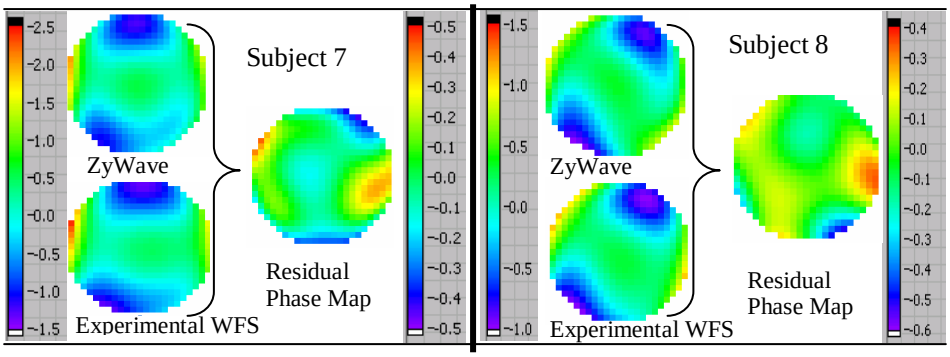

Fig. 3. Phase maps for subjects 7 and 8 over a 6 mm pupil diameter (defocus Z_2^0removed from analysis) as measured by the ZyWave and the experimental WFS. Each set of Zernike coefficients are subtracted from each other and the residual Zernike coefficients are used to reconstruct the residual phase map shown. The colour scales represent wavefront phase (microns) and are consistent for each pair of phase maps but reduced for the residual phase maps to allow detail to be discernable.

The mean residual Zernike coefficients of the 21 eyes are shown in Table 1 for a 6 mm pupil diameter. The mean residual coefficients for modes Z_3^1, Z_4^0, and Z_4^4, show a greater

#81814 - $15.00 USD Received 3 Apr 2007; revised 10 May 2007; accepted 25 May 2007; published 31 May 2007

variation between the two instruments compared to their fellow modes (in each particular order) and may indicate a calibration difference in one or both of the aberrometers. Measurements of these modes by the experimental WFS for should be interpreted with caution until a comprehensive calibration study is performed.

Table 1. Mean residual Zernike coefficients (21 eyes) for a 6mm pupil diameter (defocus Z_2^0 removed).

Z_n^m	Z_2^{-2}	Z_2^2	Z_3^{-3}	Z_3^{-1}	Z_3^1	Z_3^3	Z_4^{-4}	Z_4^{-2}	Z_4^0
Mean residual coefficient (microns)	-0.04	-0.08	0.01	-0.04	0.10	0.00	0.00	-0.02	-0.09
Z_n^m	Z_4^2	Z_4^4	Z_5^{-5}	Z_5^{-3}	Z_5^{-1}	Z_5^1	Z_5^3	Z_5^5	
Mean residual coefficient (microns)	0.00	0.03	-0.01	0.01	0.01	-0.01	0.00	0.00	

Overall, the results of the pilot study provide confidence that the experimental WFS measurements are comparable to those of a commercial aberrometer. The general shape and magnitude of the phase maps are in reasonable agreement (Fig. 2 and Fig. 3). Although the pilot study indicated that coefficients for some specific modes should be interpreted with caution, the random patterns and low amplitudes we observed in the shape of the residual phase maps for the 21 eyes in the pilot study indicate that there is no significant systematic error or bias in our experimental WFS compared to that of the commercial aberrometer. Small subject-dependent variations of ocular aberrations would be expected to occur between measurements obtained with the two instruments. The fixation target used by the Zywave (scene of Mt Fuji) could potentially cause variability in subject alignment during measurements, and it is also possible that subjects didn't actually fixate on the optical axis of the ZyWave. These limitations are likely to have contributed to the differences in aberration measurements of the two instruments. Note that the ZyWave uses a laser source with wavelength 785 nm while the experimental WFS uses a 677 nm laser source. The variation of wavefront aberrations with wavelength (except for defocus term) should not give any noticeable offset in view of the small wavelength difference (108 nm) and nearly stationary nature of high order aberrations in the near infrared region [16, 17].

The second part of the pilot study investigated the repeatability of our experimental WFS and the ZyWave. Multiple measurements with each aberrometer were performed on an experienced observer within the subject group. The same procedures as described for the first part of the pilot study were followed, except that ten measurements were performed with each aberrometer. Between each measurement the subject rested momentarily and withdrew from the headrest. All results of the pilot study (part 2) are reported for a 6 mm pupil diameter and include defocus Z_2^0. The highest standard deviation of any individual Zernike coefficient (2^{nd} to 5^{th} order) was 0.05 microns (experimental WFS) and 0.08 microns (ZyWave). The standard deviation of the total wavefront RMS (2^{nd} to 5^{th} order) was 0.11 microns (experimental WFS), and 0.13 microns (ZyWave). The standard deviation of the higher order wavefront RMS (3^{rd} to 5^{th} order) was 0.05 microns (experimental WFS), and 0.07 microns (ZyWave). The pilot study provides confidence in the repeatability of our experimental WFS, demonstrating results similar to those achieved by a commercial instrument.

5. Procedure

Subjects were selected according to the criteria described in section 3. One drop of 1% Tropicamide was administered to each eye being measured and adequate time was allowed to achieve satisfactory pupil dilation and cycloplegia. The laser power of the experimental WFS was 1.2 microwatts at the eye and the CCD exposure time was 45 milliseconds.

On-axis measurements were performed on 60 eyes. Off-axis measurements were performed on 31 eyes. The same subject alignment, measurement, manual inspection and data analysis procedures that were used during the pilot study (section 4) were also used for the on-axis and off-axis measurements. For off-axis measurements, subjects were asked to fixate a

#81814 - $15.00 USD Received 3 Apr 2007; revised 10 May 2007; accepted 25 May 2007; published 31 May 2007

marker in the fixation target corresponding to a 5 degree field angle. The instrument was then realigned to the new pupil center position. Twenty images were recorded over a typical duration of 2.5 seconds for each of the four field angles investigated; 5 degrees nasal field, 5 degrees superior field, 5 degrees temporal field, and 5 degrees inferior field.

All aberration measurements were performed by the same examiner (except for one subject). Image capturing, subject instruction, and subject alignment was standardised. The most common instrument adjustments required during measurements were translations of the ingoing beam location in the corneal plane and adjustments to the diameter of the spatial filter diaphragm. Typically these adjustments were aimed at improving HS image quality by avoiding the corneal reflections. Highly aberrated eyes required the diameter of the spatial filter to be increased slightly to allow imaging of a larger point spread function of the retinal beacon.

6. Data analysis

A 6 mm pupil diameter was selected as an appropriate value to allow population results to be pooled. All results in this experiment are presented in reference to a 6 mm pupil diameter and according to accepted standards [14]. Aberration data for pupil diameters smaller than 6 mm can be obtained by performing various rescaling procedures or by masking the raw data. These transformation techniques are discussed by Neal *et al*. [18] and Lundström and Unsbo [19]. Because we are primarily interested in higher order aberrations, Zernike coefficients describing the first order aberrations of tip Z_1^{-1} and tilt Z_1^{1} , and the second order defocus mode Z_2^{0}, were removed from the reconstructed wavefronts before commencing data analysis. For the majority of subjects, aberrations of fellow eyes were measured and bilateral symmetry as demonstrated in other studies [2,3] needs to be addressed. For certain modes, bilateral symmetry of ocular aberrations results in a strong correlation between the fitted Zernike coefficients of fellow eyes. To compensate for this effect, prior to pooling Zernike coefficients for the group, all modes with an odd symmetry about the vertical axis for the left eye were converted to an equivalent set of coefficients for the right eye by a linear transform [14].

Due to the relatively small angle (5 degrees) used for off-axis wavefront measurements, we neglect the perspective elongation of the pupil shape, which becomes elliptical when observing at oblique angles. Simulations indicated this source of error was negligable compared to other noise sources in the iris-edge detection process. For larger angles that require a perspective elongation correction, a transform method of Zernike coefficients for elliptical pupils should be applied [19].

6.1. Results for on-axis measurements

The results of our on-axis study support the general observations made by the larger studies of Thibos *et al.* [2] and Porter *et al.* [3]. We observed a high degree of individual variation in ocular aberrations. The distribution of Zernike coefficients for each mode up to the 4^{th} order is shown in Fig. 4. The distributions of 5^{th} order aberration coefficients were also analyzed and they demonstrate trends very similar to the lower orders but their histograms are not shown. Most aberration modes have a mean population coefficient value very close to zero. However, due to biological variation, it is unlikely that a subject would actually have a coefficient of exactly zero for a particular mode. It is speculated that this may be evidence of the emmetropisation process extending to higher order aberrations, or evidence of an evolutionary pressure towards aberration-free vision [2]. The histograms in Fig. 4 appear reasonably symmetric suggesting that they may be successfully fitted with a Gaussian probability density function.

The distribution for spherical aberration Z_4^{0} is shown in greater detail in Fig. 5. Our study found a mean coefficient of 0.00 ± 0.16 microns for spherical aberration Z_4^{0}. Findings in other studies [2-4] show slightly positive values for the mean Z_4^{0} coefficient. It is arguable whether the value we found is a true description of an 'average' eye, or biased due to our small sample size or relatively young population (mean age 25.7 years). Recent experimental data by many authors [20-23] indicate that ocular spherical aberration gradually increases with age. It has

#81814 - $15.00 USD Received 3 Apr 2007; revised 10 May 2007; accepted 25 May 2007; published 31 May 2007

been also suggested that the crystalline lens partly compensates the spherical aberration of the cornea [24, 25]. At a younger age this compensatory mechanism seems to be more efficient, leading to a lower amount of ocular spherical aberration [26].

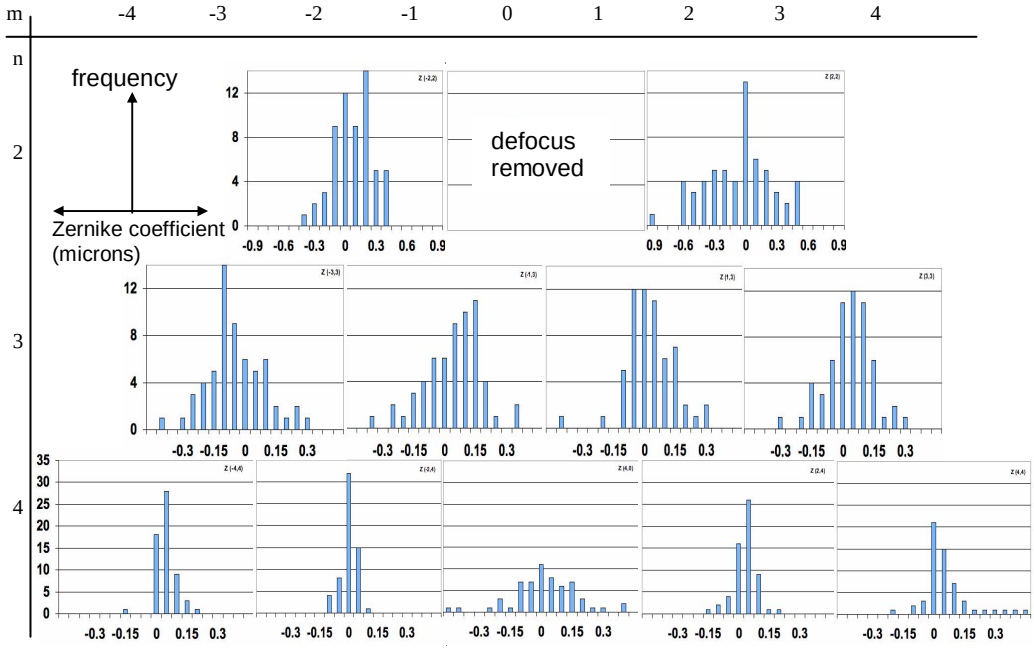

Fig. 4. The distribution of the Zernike coefficients for on-axis measurements. Note that scales are only consistent within a particular aberration order. The scales on the x- and y- axes respectively are: (-1 to +1 microns, and 0 to 14) for 2nd order, (-0.5 to +0.5 microns, and 0 to 14) for 3rd order, and (-0.5 to +0.5 microns, and 0 to 35) for 4th order. The x-axis value refers to the middle value of that particular bin.

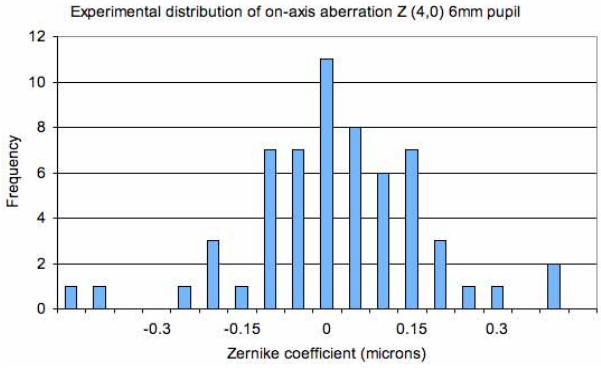

Fig. 5. Histogram displaying the distribution of spherical aberration for 60 eyes for 6 mm pupil. The x-axis value refers to the middle value of that particular bin.

Figure 6 shows the statistical distribution of coefficients for the analysed Zernike modes for on-axis measurements compared against distributions estimated from Thibos *et al.* [2].

#81814 - $15.00 USD Received 3 Apr 2007; revised 10 May 2007; accepted 25 May 2007; published 31 May 2007

The error bars represent ± 2 standard deviations. There appears to be reasonable agreement in the range and typical mean values expected in a population of normal healthy eyes. Both studies illustrate the general trend of a decreasing standard deviation of coefficient values as the aberration mode increases. The population mean aberration coefficient was close to zero for most Zernike modes. The population distributions of Zernike coefficients display similar profiles to earlier studies [2-4]. This data provides a reasonable estimate on what range of coefficients we might expect in a population of normal young eyes.

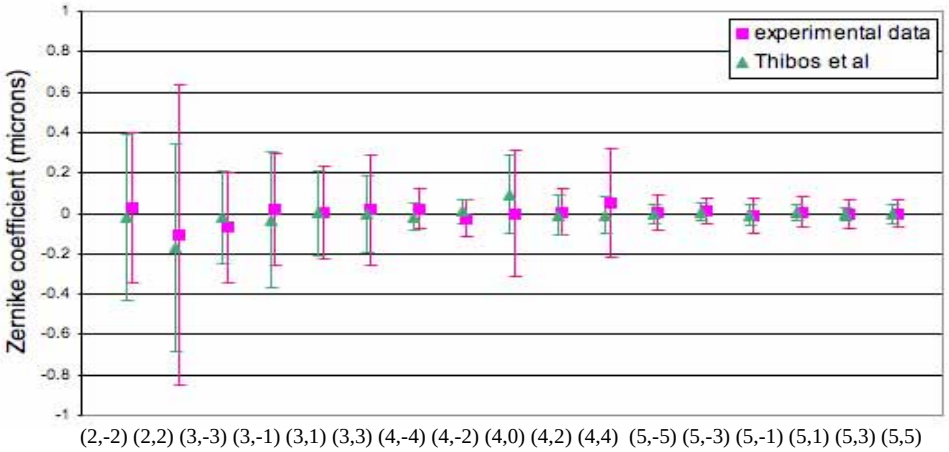

Fig. 6. The statistical distribution of Zernike coefficients over 6 mm pupil diameters for modes up to the 5th order as measured by the experimental WFS and those estimated from Thibos et al. [2]. The corresponding mean values are shown as square icons and triangle icons respectively. Error bars represent ± 2 standard deviations.

The magnitude of the higher order aberrations for any one subject was typically low compared to the dominant 2nd order aberrations. The mean higher order (3rd to 5th order) RMS wavefront error is 0.33 ± 0.17 microns. For a 6 mm pupil, 0.33 microns of defocus Z_2^0 corresponds to 0.25 DS (the traditional level of significance for refractive error correction). This may be comparable to the amount of retinal image degradation produced by 0.33 microns of higher order aberrations, assuming the MTF analysis of Guiro et al [27] can be extrapolated to infer a similar equivalency of retinal image blur would occur for the mean higher order RMS values presented. We found a slightly larger standard deviation for astigmatism Z_2^{-2} and Z_2^2 compared to data by Thibos *et al*. [2], who optimally corrected astigmatism, where as we did not. The standard deviation of the Zernike coefficient for secondary astigmatism Z_4^4 (Fig. 6) appears atypically large when measured by our experimental WFS. This suggests that secondary astigmatism Z_4^4 may have a relatively broad distribution, similar to spherical aberration Z_4^0, owing to high inter-subject variability. However, the pilot study indicated that our experimental WFS may give larger uncertainty for averaged coefficients of these modes (Z_4^0 and Z_4^4) and so this population statistic should be interpreted in a cautious manner. For 5 mm pupil diameters, Cheng *et al* found a population standard deviation of ± 0.07 microns for mode Z_4^4 (estimated from [4]). Our study found a standard deviation of ± 0.13 microns for 6 mm pupil diameters.

6.2. Results for off-axis measurements

It has been known for many years that ocular aberrations and image quality vary slowly over the central field [28]. The lowest aberrations occur on (and centered symmetrically around) the optical axis rather than the visual axis [28]. Examples of phase maps for on-axis and off-

#81814 - $15.00 USD Received 3 Apr 2007; revised 10 May 2007; accepted 25 May 2007; published 31 May 2007

axis measurements are shown in Fig. 7 for three eyes. All results are reported for 2nd to 5th order, with defocus Z_2^0 removed, over 6 mm pupils. For each eye, the general wavefront shape appears relatively similar for measurements on-axis and at most field angles. However, the colour scales reveal significant variation in amplitude between the wavefronts. Astigmatism is expected to show the most significant variation with field angle, however, at relatively small angles of 5 degrees, our results show considerable individual variation in the way ocular aberrations change across the central field. Astigmatism is not always the dominant field aberration to increase off-axis.

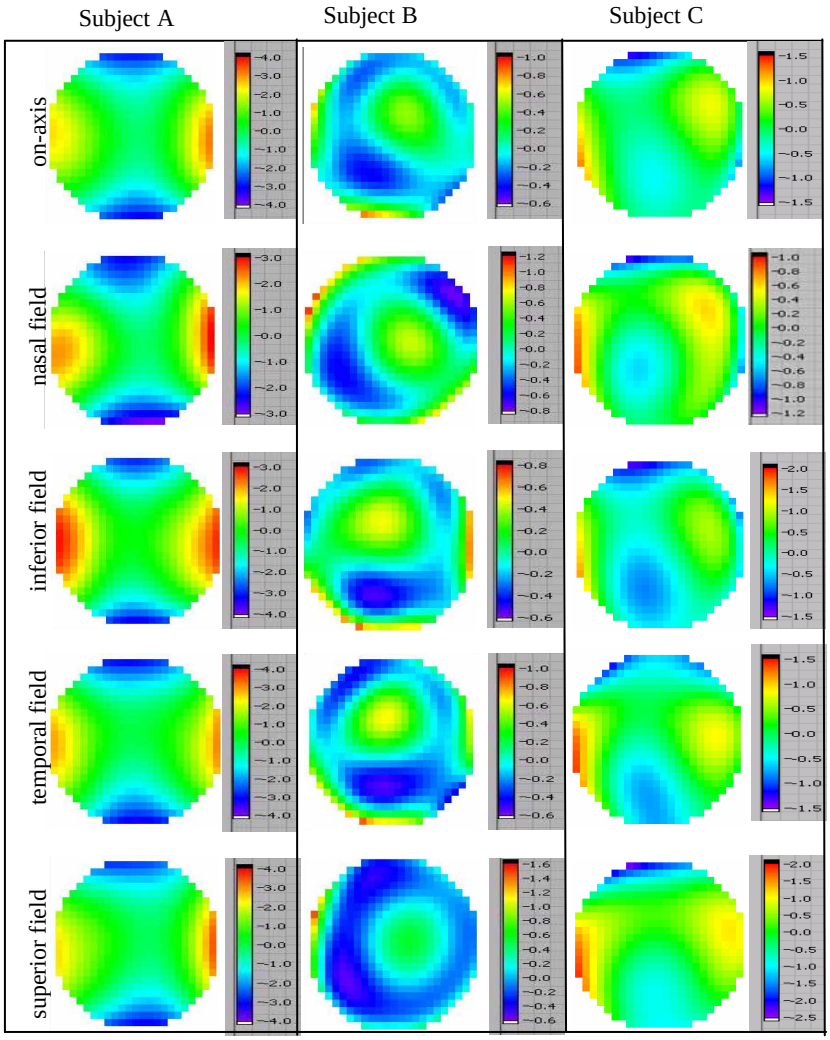

Fig. 7. Phase maps for three eyes of ocular aberrations over the central visual field for 6 mm pupils. Off-axis phase map are relative to 5 degree field angles. Note the colour scale is different between these maps due to the large variation in range between different field angles.

It is also worth noting in Fig. 7 that references to the 'temporal field' may actually be better aligned to the optical axis of the eye than 'on-axis' measurements. This is because the optical axis of the eye is typically titled by about 5 degrees temporally with respect to the line of sight (although this value has significant individual variation) [29]. Note that the optical

#81814 - $15.00 USD Received 3 Apr 2007; revised 10 May 2007; accepted 25 May 2007; published 31 May 2007

axis is defined as the line passing through or near the centers of rotation of the four optical surfaces of the eye, whereas the line of sight is defined as the axis connecting the fovea and the fixation target via the centre of the entrance pupil and exit pupil. The horizontal angular separation (angle alpha) between the line of sight and the optical axis varies from +17 degrees temporal to -2 degrees nasal [29]. Vertically, the line of sight and the optical axis are better aligned. The optical consequences of an individual's misalignment of the optical axis should be investigated in our future experiments. Modeling of the optical system of the eye based on wavefront measurements obtained off-axis at several field points might help us to find typical distribution of the angle alpha in large population.

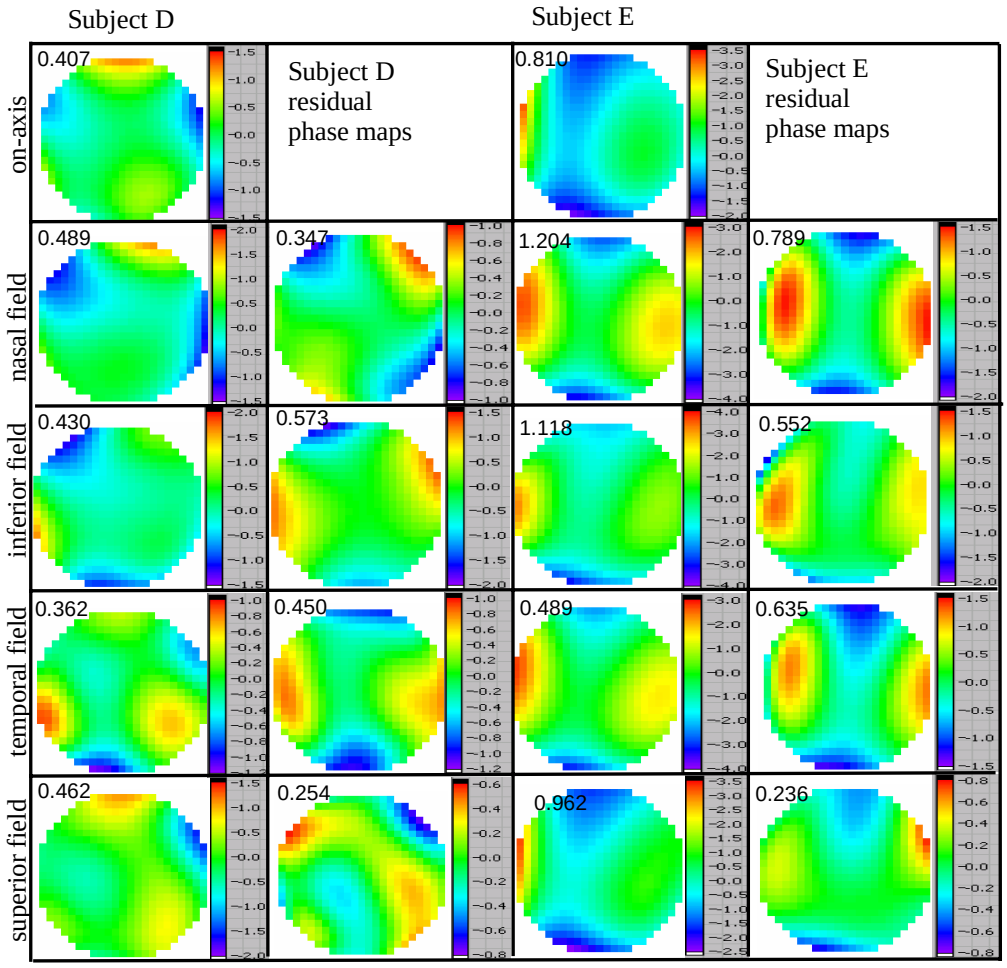

Fig. 8. On-axis, off-axis, and residual phase maps for 2 eyes. All results presented over a 6 mm pupil diameter with defocus removed. The wavefront RMS (microns) is overlaid on each phase map. The residual phase map for each off-axis field angle is generated by subtracting Zernike coefficients for on-axis aberrations from Zernike coefficients for off-axis aberrations.

Residual wavefront maps were generated for each field angles by subtracting the on-axis Zernike coefficients from those measured off-axis at the field angle. Figure 8 displays on-axis, off-axis, and residual wavefront maps for 2 eyes. All results are reported for 2nd to 5th order, with defocus removed) over 6 mm pupils. The wavefront RMS (defocus removed) in microns is overlaid on each phase map. In both of these eyes, the temporal field off-axis wavefront has a lower RMS than the on-axis wavefront, while all other off-axis wavefronts have a greater

#81814 - $15.00 USD Received 3 Apr 2007; revised 10 May 2007; accepted 25 May 2007; published 31 May 2007

RMS than the on-axis wavefront. For these two eyes, results suggest that aberrations may be minimal at some small angle in the temporal visual field rather than exactly on the line of sight. However, this is not necessarily a trend observed of all eyes. The residual RMS values are overlaid with each phase map. The lowest residual RMS value is found in the superior field for both eyes, although this is not a feature typical of all eyes. For these two eyes, when moving away from the line of sight, aberrations undergo the smallest change in the superior field direction compared to the other field directions investigated. It is important to note the large inter-subject variability we observed in the relationship between on-axis and off-axis aberrations for the 31 eyes investigated.

The tendencies displayed in Fig. 8 are not necessarily universal, however, we shall use them to illustrate two possible scenarios for aberration corrections in the eye. For subject D shown in Fig. 8 (left-hand side), removing aberrations on-axis by means of a deformable mirror conjugated to the pupil does not improve field aberrations in the temporal and inferior fields suggesting that one could probably get a better correction over the entire field by removing a common component that is averaged across the field. On the other hand, for subject E shown in Fig. 8 (right-hand side), removing aberration on axis improves also off-axis fields (except for temporal field), which can be expected, as the aberrations are more uniform across the field. It is evident that depending on the particular task one could use different regimes for field correction for example providing a minimum average residual RMS aberration in a given field region or attaining nearly uniform residual RMS aberration cross the field. Bará and Navarro [30] proposed an analytical method, which is based on the residual RMS eye aberrations, for optimal wide-field correction at the pupil.

The Zernike coefficients of the four field angles investigated were averaged for each eye and then results of each eye were pooled to produce the statistical distribution of each aberration mode shown in Fig. 9. The distribution of the average off-axis aberrations is compared against the experimental data for on-axis aberration distribution (shown also in Fig. 6). The distributions appear very similar in range and mean values. This suggests that for correction of field aberrations (by removing the component averaged across the field) one could employ a deformable mirror with a comparable stroke as in the case for aberration correction on-axis.

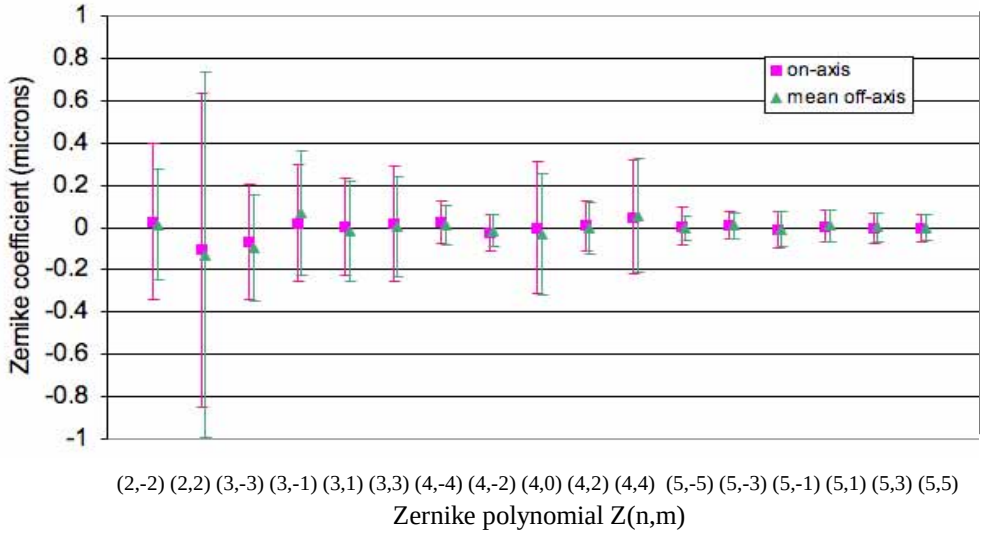

Fig. 9. The statistical distribution of Zernike coefficients measured on-axis compared to off-axis as measured by the experimental WFS for modes up to the 5th order. Mean values are represented by square and triangle icons. Error bars represent +/- 2 standard deviations.

#81814 - $15.00 USD Received 3 Apr 2007; revised 10 May 2007; accepted 25 May 2007; published 31 May 2007

7. Discussion

One of the difficulties in correcting the refractive error for a study of this kind, is that the correcting element itself (eg. trial lens) also contributes to the higher order aberrations being sensed. It is necessary to at least correct defocus (and preferably to correct astigmatism too), in both the ingoing and outgoing beams. This minimises the size of the retinal beacon, thereby improving HS spot quality, and avoids saturating the WFS. With the WFS configuration used for this experiment, satisfactory results were achieved, although the lack of refractive error correction in the ingoing beam significantly effected HS spot quality in some subjects. The ingoing laser source was positioned to bypass the Badal optometer (see Fig. 1) in an effort to avoid multiple back reflection problems. Future re-configuration of the aberrometer should allow focusing adjustments to the ingoing laser beam, while still avoiding polluting the sensing pass with either back reflections or foreign aberrations.

Using additional corrective optics conjugated to some other location away from the pupil could improve correction of the field aberrations. This approach might be different from the technique known as multiconjugate adaptive optics (MCAO), developed recently in astronomy to increase the field of view of ground-based telescopes. MCAO corrects for atmospheric turbulence, which can usually be approximated as a sequence of few discrete flat thin layers (phase screens). In contrast to the optical effects of atmospheric turbulence, the optical structure of the eye has intrinsic field aberrations as any other non-perfect imaging system. The nature of these field aberrations is quite different, for example the crystalline lens with its distributed structure of refractive index introduces aberrations continuously unlike a thin phase screens. The field dependence of low order terms and their significance to image formation are different from the aberrations caused by atmospheric turbulence. This means that correction of ocular aberrations over extended field of view might require a larger number of DMs positioned at different optical conjugates than typical number (two DMs) used in astronomical telescopes. The recent work of Bedggood *et al*. [31] confirms the limitation of MCAO approach.

8. Conclusions

This experiment took advantage of some of the unique features of the WFS constructed and the results verify its success in combining research type features in a clinically friendly instrument. The experiment helped establish the operational limits of the instrument on normal eyes, and the experience and feedback gained from this first real clinical test of the instrument has provided insight into where the potential research strengths of the instrument design lay and what minor modifications might best be adapted to correct any operational oversights.

We intend to use our results for developing subject-specific wide field schematic eye models incorporating a gradient index lens [12]. It is hoped that this statistical data would aid future designs for multi-directional ocular adaptive optics systems to achieve wide-field high resolution retinal images.

Acknowledgments

This research is funded by a Science Foundation Ireland grant No. SFI/01/PI.2/B039C and Dublin Institute of Technology.

#81814 - $15.00 USD Received 3 Apr 2007; revised 10 May 2007; accepted 25 May 2007; published 31 May 2007